On the Implementation of the Self-Interaction Corrected Local Spin Density Approximation for d- and f-Electron Systems

W. M. Temmerman[1], A. Svane[2], Z. Szotek[1], H. Winter[3], and S. V. Beiden[4]

[1] Daresbury Laboratory, Daresbury, Warrington, WA4 4AD, UK
[2] Institute of Physics and Astronomy, University of Aarhus, DK-8000 Aarhus C, Denmark
[3] Forschungszentrum Karlsruhe, INFP, Postfach 3640, Karlsruhe, Germany
[4] Department of Physics, University of Sheffield, Sheffield, UK and Department of Physics, University of West Virginia, Morgantown, West Virginia 26506-6315, USA

Abstract. The ab-initio self-interaction corrected (SIC) local-spin-density (LSD) approximation is elaborated upon, with emphasis on the ability to describe localization phenomena in solids. Two methods for minimizing the SIC–LSD total energy functional are considered, one using an unified Hamiltonian for all electron states, thus having the advantages of Bloch's theorem, the other one employing an iterative scheme in real space. Moreover, an extension of the formalism to the relativistic case is discussed. Results for NiO, cerium and cerium compounds are presented. For NiO a significant charge transfer gap is produced, in contrast to the near vanishing band gap seen in the LSD approximation. Also, the magnetic moment is larger in the SIC–LSD approach than in the LSD approach. For the cerium compounds, the intricate isostructural phase transitions in elemental cerium and cerium pnictides may be accurately described. A sizeable orbital moment for elemental cerium metal is obtained which, upon lattice expansion, is seen to reach the atomic limit.

1 Introduction

Density Functional Theory (DFT)[1] is a very powerful tool for performing *ab initio* electronic structure calculations for complex systems. It provides an exact mapping of a many–body electron problem which occurs in solids onto a one–electron problem. Instead of considering, for N interacting electrons in an external potential $V_{\rm ext}(\mathbf{r})$, the 3N-dimensional Schrödinger equation for the wavefunction $\Psi(\mathbf{r}_1, \mathbf{r}_2, \mathbf{r}_3, ..., \mathbf{r}_N)$, DFT expresses this many–body problem in terms of the electronic density distribution $n(\mathbf{r})$ and a universal exchange and correlation functional of the density, $E_{xc}[n]$. The task of solving the many–body problem is then reduced to finding sufficiently accurate expressions for $E_{xc}[n]$ and then solving the relevant one–electron Schrödinger equation with an effective potential of which the exchange–correlation potential is a prominent part. Generalizing DFT to the spin-polarised case, the spin-density functional theory (SDFT) allows to study magnetic systems, where the magnetization density is the order parameter of the theory, and appears explicitly in the exchange–correlation energy functional, i.e. , $E_{xc}[n, \mathbf{m}]$.

H. Dreyssé (Ed.): Workshop 1998, LNP 535, pp. 286–312, 1999.

The local-spin-density (LSD) approximation to SDFT provides a simple and rather successful scheme[2]. This is owing to a simple and practical approximation for $E_{xc}[n, \mathbf{m}]$, where the exchange and correlation energy of the electrons in the solid is expressed in terms of the exchange–correlation energy per particle, $\varepsilon_{xc}(n, \mathbf{m})$, of a homogeneous electron gas of homogeneous density n and magnetization $\mathbf{m}$. Specifically, in each point in space the electrons present are assumed to contribute an exchange–correlation energy given as if they were in a homogeneous electron gas at the local density $n(\mathbf{r})$ and $\mathbf{m}(\mathbf{r})$:

$$E_{xc}^{\mathrm{LSD}}[n, \mathbf{m}] \equiv \int n(\mathbf{r}) \varepsilon_{xc}(n(\mathbf{r}), \mathbf{m}(\mathbf{r})) d\mathbf{r},$$

The simple function $\varepsilon_{xc}(n, \mathbf{m})$ is known with great precision, and hence allows for an accurate determination of the ground state energies and charge densities of any system.

The LSD is a highly accurate approximation for systems where the electrons are delocalized and travel 'fast' through the solid. However, when the 'static' electron-electron interactions become so strong that some electrons get localized on atomic sites in the solid, the LSD, as well as its gradient corrections, fail to describe the correct groundstate. This obviously means that the $E_{xc}[n, \mathbf{m}]$ can not anymore be adequately represented by the LSD. For when the electron slows down upon localization it starts responding to a different potential than the effective LSD potential.

One of the most prominent examples where electron correlations are too strong to be properly treated within LSD is the high-temperature superconductors, for which LSD fails to produce the antiferromagnetic and semiconducting ground states of the generic La_2CuO_4 and $YBa_2Cu_3O_6$ compounds [3]. Other examples are the $3d$ transition metal oxides MnO, FeO, CoO and NiO, which are Mott insulators characterized by localized d-electrons [4,5]. These materials have antiferromagnetic order and large energy gaps although the metal d-shell is incompletely filled. The LSD approximation does reveal the magnetic ordering but with somewhat too small magnetic moments and vanishing (for FeO and CoO) or very small (for MnO and NiO) gaps [6]. In addition, the persistence of the magnetic moments above the Néel temperature is difficult to explain in the Slater-Stoner picture of magnetism inherent in the LSD band picture. The failure of LSD in producing the correct gaps may be traced to the fact that the LSD eigenenergies do not have built in the large on-site Coulomb repulsion, which characterizes the separation between occupied and unoccupied states [5,7,8]. LSD also fails to give a physically correct picture of trivalent cerium compounds, which are characterized by each Ce atom having a localized $f-$electron. Cerium is the first element of the Periodic Table to accomodate an $f-$electron. This $4f-$electron is peculiar in being spatially localized with a radial extent much smaller than that of the $5s$ and $5p$ semicore states, yet having an energy in the region of the valence $6s$ and $5d$ electrons. Cerium metal has been widely studied over the years, both experimentally and theoretically, mostly due to its famous isostructural $\gamma \rightarrow \alpha$ phase transition, occuring at a pressure of $\sim$8 kbar. This phase transition is believed to occur as a consequence of a change in bonding

properties of the $f-$electrons. In the (high–volume) γ phase the $f-$electrons behave as non–bonding localized moments with a Curie–Weiss type susceptibility, while the (low–volume) α-phase is characterized by the f-electrons taking more active part in the cohesion, either by hybridizing into the Bloch states, as envisaged in the Mott transition model [9], or by forming a complicated Kondo lattice groundstate [10]. In an LSD calculation the total energy minimum is found in the region somewhat below the α phase volume. Upon expansion of the lattice, the $\gamma \rightarrow \alpha$ transition is signalled by the onset of magnetization around the observed lattice parameter for the γ phase [11]. The calculated pressure is much too negative, however, since the f-electrons still contribute significantly to the cohesion in the spin-polarized phase. The loss of cohesion upon localization has been successfully described within the LSD in cases where the f-shell is half filled, as in americium [12].

The concept of an electron being 'localized' is not particularly well-defined. In a solid a periodic array of deep core states is equally well described by a set of atom centered Wannier states or by **k**-dependent Bloch functions. A unitary transformation connects the two representations, but the physical picture of a core state is that of a localized wavefunction. The observation of multiplet effects in photoemission experiments on $3d$ monoxides and rare-earth systems seems to suggest that the local description is most appropriate for such systems. On the other hand the great success of modern solid state theory in explaining most conventional metals, semiconductors and insulators leaves little doubt that the Bloch picture of normal valence electrons is the more fruitful one.

The Hubbard model [13] has often been used to describe materials where localization phenomena occur. The substantial Coulomb correlations on particular atoms, say on a Ni d^8 ion in NiO, induce an orbital polarization [5], which may well be described already in a mean-field treatment of the Hubbard model, as has been shown in the LDA+U approach [8,14]. However, the 'localizing' Hubbard term is usually too large to facilitate an accurate description of delicate localization-delocalization transitions, as for example observed in rare-earth and actinide systems.

Another way of taking into account the 'slowing down' of an electron upon localization is to consider orbital–dependent functionals, $E_{xc}[\{\psi_\alpha\}]$, where $\{\psi_\alpha\}$ is a set of one–electron orbitals with the orbital index α. These functionals are a possible evolution on the LSD and can be considered as a basis of the orbital–dependent DFT. They can be treated as the starting point for new approximations to DFT. The self–interaction–corrected LSD (SIC-LSD) is one such approximation [15]. It is based upon the observation that localized orbitals in the LSD give rise to an error due to a spurious self–interaction contained in the effective one–electron potential. This error increases the more localized the orbital becomes. For a 'fast' electron, however, the self-interaction is negligible or zero. The SIC-LSD energy functional is constructed from the LSD functional by explicit subtraction of the self-interaction term from the E_{xc}^{LSD} term. As we will demonstrate in this paper the SIC-LSD functional allows for an improved

treatment of the electron correlations, and is more adequate than the LSD for systems where both localized and delocalized electrons are present.

Solids where both localized and delocalized electrons are present give rise to some of the most facinating phenomema in solid state physics. They include the heavy fermion compounds and their complicated phase diagrams at low temperatures, the still unexplained phenomenon of the high T_c superconductivity, the observation of collossal–magneto resistance, with its potentially wide ranging technological applications. The theoretical investigations have usually been confined to either studies of generic model Hamiltonians which allow for a very accurate treatment of the electron–electron interactions, or materials specific LSD calculations with a not fully satisfactory treatment of the 'static' electron–electron correlations.

As already mentioned, the basic assumption in the SIC–LSD is that 'localized' electron states experience a different potential from that of the normal delocalized valence electrons. One may argue for such a differentiation by thinking in terms of Wigner delay times of electrons on a particular atom [16]. If an electron resides on a given atom for a long time the local electronic structure of the atom accomodates to the presence of the added electron, while a fast electron has no influence on the effective structure of that atom. This picture is implemented by assuming a fast ('delocalized') electron to experience an effective potential as given by the LSD approximation, while a slow ('localized') electron experiences the LSD potential corrected for the self-interaction of the electron in question. Taking the d^8 configuration of a Ni ion in NiO as an example, one of the 8 d-electrons residing on a particular atomic site experiences Coulomb interactions with 7 other d-electrons. On the other hand, a conduction electron injected into a perfect NiO crystal will be made out of excited states, which ride on top of an array of Ni d^8 ions, and therefore Coulomb interacts with all the 8 d-electrons. That the LSD is adequate for describing the 'fast' electron is validated by the great success of this approach in describing the bonding properties of conventional metals. This picture is still very idealized, since the transition from localized to delocalized must be a gradual one. The added electron in NiO still may show some localized characteristics, and the ground state electrons do sometimes show **k**-dependent dispersions. However, one may be able to distinguish phases of solids being either predominantly 'localized' or predominantly 'delocalized', which will be the subject of the present paper.

In Section II the general formalism of the SIC–LSD approximation will be discussed, and in Sections III and IV two implementations of the approach into *ab-initio* linear-muffin-tin orbitals (LMTO)[17] band structure codes will be outlined. Section V is devoted to a relativistic extension of the formalism, while in Section VI we concentrate on applications. Section VII concludes the paper.

2 The SIC Formalism

In the LSD all electrons feel the same mean-field single particle potential, V^{LSD}, and the same magnetic field, $\mathbf{B}_{\mathit{eff}}$, which depends on the total charge density, n,

and magnetization density, $\mathbf{m}$. The LSD energy functional, E^{LSD}, has the form:

$$E^{\mathrm{LSD}} = E_{\mathrm{kin}} + U[n] + \int d\mathbf{r}\; V_{\mathrm{ext}}(\mathbf{r}) n(\mathbf{r}) + E_{xc}^{\mathrm{LSD}} + \int d\mathbf{r}\; \mathbf{m}(\mathbf{r}) \cdot \mathbf{B}_{\mathrm{ext}}(\mathbf{r}) \tag{1}$$

with

$$\begin{aligned} E_{\mathrm{kin}} &= \sum_{\alpha} \langle \psi_\alpha | \hat{T} | \psi_\alpha \rangle \\ U[n] &= \frac{1}{2} \int d\mathbf{r} V_H(\mathbf{r}) n(\mathbf{r}) \\ V_{\mathrm{H}}(\mathbf{r}) &= \int d\mathbf{r}' \frac{2n(\mathbf{r}')}{|\mathbf{r} - \mathbf{r}'|} \\ V_{\mathrm{ext}}(\mathbf{r}) &= -\sum_{\mathbf{T},\tau} \frac{2Z_\tau}{|\mathbf{T} + \boldsymbol{\tau} - \mathbf{r}|} \\ E_{xc}^{\mathrm{LSD}}[n, \mathbf{m}] &= \int d\mathbf{r}\; n(\mathbf{r})\; \varepsilon_{xc}(n(\mathbf{r}), \mathbf{m}(\mathbf{r})). \end{aligned}$$

Here, $\hat{T}$ is a kinetic energy operator, and the ψ_α's are the one-electron wavefunctions which in the nonrelativistic as well as the scalar relativistic case are two-component spinors. $\mathbf{B}_{\mathrm{ext}}(\mathbf{r})$ is the external magnetic field, Z_τ is the atomic number of site τ, $\mathbf{T}$ is a lattice translation vector of the Bravais lattice, and $\boldsymbol{\tau}$ is the postion vector of site τ in the unit cell. n and $\mathbf{m}$ may be expressed in terms of the ψ_α's in the usual way

$$\begin{aligned} n(\mathbf{r}) &= \sum_{\alpha} n_\alpha(\mathbf{r}) = \sum_{\alpha}\; \psi_\alpha^*(\mathbf{r}) \psi_\alpha(\mathbf{r}) \\ \mathbf{m}(\mathbf{r}) &= \sum_{\alpha} \mathbf{m}_\alpha(\mathbf{r}) = \sum_{\alpha}\; \psi_\alpha^*(\mathbf{r}) \boldsymbol{\sigma} \psi_\alpha(\mathbf{r}), \end{aligned} \tag{2}$$

with $\boldsymbol{\sigma}$ being the spin operator.

Minimizing the above energy functional by taking the functional derivative of E^{LSD} with respect to ψ_α^*, leads to the single particle wave equation of the form

$$h^{\mathrm{LSD}}(\mathbf{r}) \psi_\alpha(\mathbf{r}) \;=\; (\; T + V^{\mathrm{LSD}}(\mathbf{r}) + \boldsymbol{\sigma} \cdot \mathbf{B}^{\mathrm{LSD}}(\mathbf{r}) \;)\; \psi_\alpha(\mathbf{r}) = \varepsilon_\alpha\; \psi_\alpha(\mathbf{r}), \tag{3}$$

with

$$\begin{aligned} V^{\mathrm{LSD}}(\mathbf{r}) &= V_H(\mathbf{r}) + V_{xc}^{\mathrm{LSD}}(\mathbf{r}) \\ V_{xc}^{\mathrm{LSD}}(\mathbf{r}) &= \frac{\delta E_{xc}^{\mathrm{LSD}}[n, \mathbf{m}]}{\delta n(\mathbf{r})} \\ \mathbf{B}^{\mathrm{LSD}}(\mathbf{r}) &= \mathbf{B}_{\mathrm{ext}}(\mathbf{r}) + \mathbf{B}_{xc}^{\mathrm{LSD}}(\mathbf{r}) \\ \mathbf{B}_{xc}^{\mathrm{LSD}}(\mathbf{r}) &= \frac{\delta E_{xc}^{\mathrm{LSD}}[n, \mathbf{m}]}{\delta \mathbf{m}(\mathbf{r})}. \end{aligned} \tag{4}$$

As discussed in the introduction the LSD successfully describes many solid state properties, but suffers from a deficiency caused by the spurious self-interaction (SI). Namely, such contributions to $E^{\rm LSD}$ as $U[n]$, $E_{xc}^{\rm LSD}$, and $\mathbf{B}_{xc}^{\rm LSD}$ contain spurious self-interactions of the single particle charges, n_α, and magnetic moments, $\mathbf{m}_\alpha$, which do not cancel. The exact SDFT energy functional does not contain any self-interaction, and also in some existing approximations, e.g., the Hartree-Fock theory, the SI terms cancel out. Of course, due to its great merits, it does not seem justified to discard the LSD altogether in cases where this inherent self-interaction matters. Instead, in such cases, it is sufficient to augment LSD with terms removing this deficiency. The resulting approach, the self-interaction corrected LSD (SIC-LSD) formalism,[15] is defined by the following functional

$$E^{\text{SIC-LSD}} \;=\; E^{\rm LSD} \;+\; E^{\rm SIC}, \tag{5}$$

with

$$\begin{aligned}
E^{\rm SIC} &= -\sum_\alpha e_\alpha[n_\alpha,\mathbf{m}_\alpha] = -\sum_\alpha (\; U[n_\alpha] \;+\; E_{xc}^{\rm LSD}[n_\alpha,\mathbf{m}_\alpha]\;)\\
U[n_\alpha] &= \frac{1}{2}\int d\mathbf{r}\; n_\alpha(\mathbf{r}) V_{H,\alpha}(\mathbf{r})\\
V_{{\rm H},\alpha} &= \int d\mathbf{r}'\;\frac{2n_\alpha(\mathbf{r}')}{|\mathbf{r}-\mathbf{r}'|}.\\
E_{xc}^{\rm LSD}[n_\alpha,\mathbf{m}_\alpha] &= \int d\mathbf{r}\; n_\alpha(\mathbf{r})\varepsilon_{xc}(n_\alpha(\mathbf{r}),\mathbf{m}_\alpha(\mathbf{r}))
\end{aligned}$$

The corresponding single-particle wave equation, obtained by taking the functional derivative of $E^{\text{SIC-LSD}}$ with respect to ψ_α^*, reads

$$(\; h^{\rm LSD}(\mathbf{r}) \;+\; w_\alpha^{\rm SIC}(\mathbf{r})\;)\;\psi_\alpha(\mathbf{r}) \;=\; \sum_{\alpha'}\lambda_{\alpha,\alpha'}\;\psi_{\alpha'}(\mathbf{r}), \tag{6}$$

with $h^{\rm LSD}$ given in Eq. (3) and

$$\begin{aligned}
w_\alpha^{\rm SIC} &= v_\alpha^{\rm SIC} \;+\; \boldsymbol{\sigma}\cdot\mathbf{b}_\alpha^{\rm SIC}\\
v_\alpha^{\rm SIC} &= -(\; V_{H,\alpha}(\mathbf{r}) + V_{xc,\alpha}^{\rm LSD}(\mathbf{r})\;)\\
v_{xc,\alpha}^{\rm LSD}(\mathbf{r}) &= \frac{\delta E_{xc}^{\rm LSD}[n_\alpha,\mathbf{m}_\alpha]}{\delta n_\alpha(\mathbf{r})}\\
\mathbf{b}_\alpha^{\rm SIC}(\mathbf{r}) &= -\frac{\delta E_{xc}^{\rm LSD}[n_\alpha,\mathbf{m}_\alpha]}{\delta \mathbf{m}_\alpha(\mathbf{r})}.
\end{aligned}$$

Note that the problem of finding the single-particle states is now complicated by the fact that each state sees a different potential, $w_\alpha^{\rm SIC}$. Instead of determining the energy eigenvalues, it is therefore necessary to evaluate the Lagrange multipliers matrix, λ, to ensure orthonormality within the set of states ψ_α. Furthermore, we should remark that in contrast to $E^{\rm LSD}$, $E^{\text{SIC-LSD}}$ is not invariant with respect to unitary transformations in the space of the states ψ_α: Suppose

we perform a unitary transformation among the occupied orbitals specified by the matrix $U = 1 + i(dS)$, with $(dS)_{\alpha_1,\alpha_2} = \varepsilon, (dS)_{\alpha_2,\alpha_1} = \varepsilon^*$. Then the states ψ_{α_1}, and ψ_{α_2} change to first order in ε by $i\varepsilon\psi_{\alpha_2}$ and $i\varepsilon^*\psi_{\alpha_1}$, respectively. Using the definition of $w_\alpha^{\rm SIC}$ (Eq. (6)), we find the first order change of $E^{\rm SIC}$ to be: $dE^{\rm SIC} = i\varepsilon\ \langle\psi_{\alpha_1}|w_{\alpha_1}^{\rm SIC} - w_{\alpha_2}^{\rm SIC}|\psi_{\alpha_2}\rangle\ +\ c.c.$. If we intend to study the ground state properties we should therefore choose the states ψ_α so that they minimize $E^{\rm SIC}$ with respect to all unitary transformations, that is to say, they fulfil the so-called localization criterion

$$\langle\psi_{\alpha_1}|w_{\alpha_1}^{\rm SIC} - w_{\alpha_2}^{\rm SIC}|\psi_{\alpha_2}\rangle\ =\ 0. \tag{7}$$

It appears that the SIC-potentials $w_\alpha^{\rm SIC}$ are significant for those states whose charges are localized in space. Thus the importance of SI corrections for atoms, molecules and core electrons in solids seems obvious. However, our main interest concentrates on the valence electrons in periodic solids. If extended Bloch states are used to describe these electrons, the corresponding $w_\alpha^{\rm SIC}$'s turn out to be negligible. If, on the other hand, spatially localized states are used the $w_\alpha^{\rm SIC}$ may be an attractive potential contribution of considerable size. In the remainder of this and the following section we will describe one method of solving the SIC-LSD energy minimization problem of Eq. (6), while section IV describes another yet equivalent procedure.

In what follows we assume that the electronic system in question may be described by Wannier states Φ, each centered around some atom τ in some unit cell, displaced from the central unit cell by the lattice translation vector $\mathbf{T}$. For some of these states, defined by ϕ_α with $\alpha = (m, \mathbf{T})$, the SI-corrections are assumed to be negligible, while for the others, defined by ψ_β with $\beta = (n, \mathbf{T})$, the SI-corrections have to be taken into account explicitly. Indices n and m thus enumerates the Wannier states within the unit cell. For a periodic solid we assume a periodic repetition of localized states, i. e.,

$$\psi_{n,\mathbf{T}}(\mathbf{r}) = \psi_{n,\mathbf{T}=0}(\mathbf{r} - \mathbf{T}) = \psi_n(\mathbf{r} - \mathbf{T}). \tag{8}$$

$$\phi_{m,\mathbf{T}}(\mathbf{r}) = \phi_{m,\mathbf{T}=0}(\mathbf{r} - \mathbf{T}) = \phi_m(\mathbf{r} - \mathbf{T}). \tag{9}$$

The same symmetry applies to the SIC-potential of state $\psi_{n,\mathbf{T}}$:

$$w_{n,\mathbf{T}}^{\rm SIC}(\mathbf{r}) = w_{n,\mathbf{T}=0}^{\rm SIC}(\mathbf{r} - \mathbf{T}) = w_n^{\rm SIC}(\mathbf{r} - \mathbf{T}), \tag{10}$$

and the Lagrange multipliers matrix as

$$\lambda_{n,\mathbf{T};n',\mathbf{T}'}\ =\ \lambda_{n;n'}(\mathbf{T} - \mathbf{T}'). \tag{11}$$

Considering the states ψ_n and ϕ_m as the elements of the column vector Φ, and their complex conjugates as the elements of the row vector $\Phi^\dagger$, Eq. (6) may be rewritten in matrix form as

$$(\ H^{\rm LSD}(\mathbf{r})\ +\ W^{\rm SIC}(\mathbf{r} - \mathbf{T})\ )\ \Phi(\mathbf{r} - \mathbf{T})\ =\ \sum_{\mathbf{T}'} \lambda(\mathbf{T} - \mathbf{T}')\ \Phi(\mathbf{r} - \mathbf{T}'). \tag{12}$$

Here, H^{LSD} and W^{SIC} are diagonal matrices, and the subblock of W^{SIC} acting on the states ϕ_m is zero. Since the λ's are chosen to make the states Φ orthonormal, the Lagrange multipliers may be expressed as the following matrix elements of the SIC-Hamiltonian

$$\lambda(\mathbf{T}-\mathbf{T}') = \sum_{\mathbf{T}_1} \int_{\Omega_{unit}} d\mathbf{r} \Phi^{\dagger}(\mathbf{r}+\mathbf{T}-\mathbf{T}'+\mathbf{T}_1)(H^{\mathrm{LSD}}(\mathbf{r}) + W^{\mathrm{SIC}}(\mathbf{r}+\mathbf{T}_1))\Phi(\mathbf{r}+\mathbf{T}_1). \tag{13}$$

When deriving Eq. (13) we have made use of Eqs. (8) to (10). To construct the Bloch state vector, $\Psi_{\mathbf{k}}$, we form the following lattice sum

$$\Psi_{\mathbf{k}}(\mathbf{r}) \;=\; \sum_{\mathbf{T}} M^{-1}(\mathbf{k}) \;\exp(-\mathrm{i}\mathbf{k}\mathbf{T})\; \Phi(\mathbf{r}+\mathbf{T}), \tag{14}$$

while the inverse transformation is

$$\Phi(\mathbf{r}+\mathbf{T}) \;=\; \frac{1}{\Omega_{BZ}} \int d\mathbf{k}\; M(\mathbf{k}) \;\exp(\mathrm{i}\mathbf{k}\mathbf{T})\; \Psi_{\mathbf{k}}(\mathbf{r}). \tag{15}$$

Here, the $\mathbf{k}$-integration is over the Brillouin zone (BZ) whose volume is Ω_{BZ}. The unitary matrix M will be elaborated upon at a later stage. By acting from the left with the operator

$$A = \sum_{\mathbf{T}} M^{-1}(\mathbf{k}) \exp(-\mathrm{i}\mathbf{k}\mathbf{T}),$$

on the wave equation for $\Phi(\mathbf{r}+\mathbf{T})$, Eq. (12), one obtains the following wave equation for the Bloch state vector $\Psi_{\mathbf{k}}(\mathbf{r})$ with the wave vector $\mathbf{k}$:

$$(\; H^{\mathrm{LSD}}(\mathbf{r}) \;+\; V^{\mathrm{SIC}}_{\mathbf{k}}(\mathbf{r}) \;)\, \Psi_{\mathbf{k}}(\mathbf{r}) \;=\; \lambda_{\mathbf{k}}\, \Psi_{\mathbf{k}}(\mathbf{r}). \tag{16}$$

Here $V^{\mathrm{SIC}}_{\mathbf{k}}$ is a diagonal matrix whose elements, $v^{\mathrm{SIC}}_{\mathbf{k},\nu}$, are given by

$$v^{\mathrm{SIC}}_{\mathbf{k},\nu}(\mathbf{r})\Psi_{\mathbf{k},\nu}(\mathbf{r}) = \sum_{n} \sum_{\mathbf{T}} (M^{-1}(\mathbf{k}))_{\nu,n} \exp(\mathrm{i}\mathbf{k}\mathbf{T}) w^{\mathrm{SIC}}_n(\mathbf{r}+\mathbf{T}) \psi_n(\mathbf{r}+\mathbf{T}), \tag{17}$$

where the subscripts n and ν refer to bands. The Lagrange multipliers matrix, $\lambda_{\mathbf{k}}$, is defined as

$$\lambda_{\mathbf{k}} \;=\; \sum_{\mathbf{T}} \exp(\mathrm{i}\mathbf{k}\mathbf{T})\; M^{-1}(\mathbf{k})\; \lambda(\mathbf{T})\; M(\mathbf{k}). \tag{18}$$

Note that V^{SIC} has lattice translational symmetry: $V^{\mathrm{SIC}}_{\mathbf{k}}(\mathbf{r}+\mathbf{T}) = V^{\mathrm{SIC}}_{\mathbf{k}}(\mathbf{r})$, due to the symmetry of the Bloch states: $\Psi_{\mathbf{k},\nu}(\mathbf{r}+\mathbf{T}) = \exp(\mathrm{i}\mathbf{k}\mathbf{T})\Psi_{\mathbf{k},\nu}(\mathbf{r})$. In practical applications $v^{\mathrm{SIC}}_{\mathbf{k},\nu}$ is chosen to be nonzero only for the bands which are expected to be extremely narrow, i.e. having well localized Wannier states. We shall call

the states corresponding to such bands the SI corrected Bloch states, and label them by c, while the rest of states shall be referred to as the non-SI corrected Bloch states, and labelled by nc.

It is straightforward to write $\mathrm{E}^{\mathrm{LSD}}$ in the usual way in terms of the Bloch states, $\Psi_{\mathbf{k}}$, while $\mathrm{E}^{\mathrm{SIC}}$ is expressed through the Wannier states $\psi_n(\mathbf{r}-\mathbf{T})$ as:

$$E^{\mathrm{SIC}} = -\sum_{n,\mathbf{T}} e_n[n_n, \mathbf{m}_n]. \tag{19}$$

Due to the translational symmetry of the localized states, and making use of Eqs. (8) to (10), the localization criterion, Eq. (7), takes the following form

$$\sum_{\mathbf{T}} \int_{\Omega_{unit}} d\mathbf{r}\ \psi^*_{n_1}(\mathbf{r}+\mathbf{T})\ (w_{n_1}(\mathbf{r}+\mathbf{T}) - w_{n_2}(\mathbf{r}+\mathbf{T}+\mathbf{T}_1-\mathbf{T}_2))$$
$$\psi_{n_2}(\mathbf{r}+\mathbf{T}+\mathbf{T}_1-\mathbf{T}_2) \ = \ 0. \tag{20}$$

This relation is valid for any pair of states ψ_{n_1} and ψ_{n_2}, and arbitrary translation lattice vectors $\mathbf{T}_1$, $\mathbf{T}_2$. Here the integration is over the volume of the central unit cell. By inserting this relation into Eq. (13) it is easy to see that the subblock of the Lagrange multipliers matrix λ, built by the SIC-corrected localized states ψ_n, is hermitian

$$\lambda_{n1,n2}(\mathbf{T}_1 \ - \mathbf{T}_2\ ) \ = \ \lambda^*_{n2,n1}(\mathbf{T}_2 \ - \ \mathbf{T}_1). \tag{21}$$

Finally, it remains to define the matrix $\mathrm{M}(\mathbf{k})$ introduced in Eq. (14). The requirement is that this matrix, via Eq. (15), generates well localized states, ψ_n, that satisfy the wave equation (12), and for which the SI corrections are significant. The following expression turned out to meet such requirements

$$M(\mathbf{k}) \ = \ U\ M^{(1)}(\mathbf{k}) \tag{22}$$

with

$$(M^{(1)}(\mathbf{k}))_{\nu,\nu'} \ = \ N_\nu(\mathbf{k}) \int_\Omega d\mathbf{r}\ \Psi^*_{\mathbf{k},\nu'}(\mathbf{r})\ \Psi_{\mathbf{k}=0,\nu}(\mathbf{r}) \tag{23}$$

and

$$N_\nu(\mathbf{k}) \ = \ (\sum_{\nu'} |\int_\Omega d\mathbf{r}\Psi^*_{\mathbf{k},\nu'}(\mathbf{r})\Psi_{\mathbf{k}=0,\nu}(\mathbf{r})|^2)^{-1/2}. \tag{24}$$

Here the integration is over the volume Ω, obtained by applying all symmetry operations of the crystalline point group to the unit cell. The matrix U is determined numerically so that the localized states ψ_n are orthonormal and fulfil the localization criterion (Eq. (20)).

3 The Unified Hamiltonian Approach

In practical applications we have to iterate Eqs. (4), (6) and (16) to (18) to self-consistency. In particular, the Lagrange multipliers matrix, $\lambda_{\mathbf{k}}$, has to be evaluated to ensure the orthonormality of the Bloch states, $\Psi_{\mathbf{k}}$. An alternative method, developed in relation to the Hartree-Fock theory, consists in solving the eigenvalue problem for a hermitian operator, $h_{u,\mathbf{k}}$, the so-called unified Hamiltonian

$$h_{u,\mathbf{k}} \, |\Psi_{\mathbf{k},\nu}\rangle \; = \; \varepsilon_{\mathbf{k},\nu} \, |\Psi_{\mathbf{k},\nu}\rangle. \tag{25}$$

To define $h_{u,\mathbf{k}}$ appropriate for the SIC-LSD method[18] we introduce the projection operators, $P_{\mathbf{k}}$, onto the subspaces of the SI corrected Bloch states, $\Psi_{\mathbf{k},c}$, and the projection operators, $Q_{\mathbf{k}}$, onto the subspace of the non-SI corrected Bloch states, $\Psi_{\mathbf{k},nc}$, namely

$$\begin{aligned} P_{\mathbf{k}} \; &= \; \sum_{c} P_{\mathbf{k},c} \; = \; \sum_{c} |\Psi_{\mathbf{k},c}\rangle \, \langle \Psi_{\mathbf{k},c}| \\ Q_{\mathbf{k}} \; &= \; \sum_{nc} Q_{\mathbf{k},nc} \; = \; \sum_{nc} |\Psi_{\mathbf{k},nc}\rangle \, \langle \Psi_{\mathbf{k},nc}|. \end{aligned} \tag{26}$$

Subsequently, $h_{u,\mathbf{k}}$ is defined as

$$\begin{aligned} h_{u,\mathbf{k}} \; = \; h^{\mathrm{LSD}} \; - \sum_{c,c';(c\neq c')} P_{\mathbf{k},c} \, h^{\mathrm{LSD}} \, P_{\mathbf{k},c'} + \sum_{c} P_{\mathbf{k},c} \, v^{\mathrm{SIC}}_{\mathbf{k},c} \, P_{\mathbf{k},c} \\ + Q_{\mathbf{k}} \sum_{c} v^{\mathrm{SIC}}_{\mathbf{k},c} \, P_{\mathbf{k},c} \; + \sum_{c} P_{\mathbf{k},c} \, v^{SIC\dagger}_{\mathbf{k},c} \, Q_{\mathbf{k}} \end{aligned} \tag{27}$$

or alternatively as

$$\begin{aligned} h_{u,\mathbf{k}} \; = \; h^{\mathrm{LSD}} \; + \sum_{c} v^{\mathrm{SIC}}_{\mathbf{k},c} \, P_{\mathbf{k},c} \\ - \sum_{c,c';(c\neq c')} P_{\mathbf{k},c} \, (h^{\mathrm{LSD}} + v^{\mathrm{SIC}}_{\mathbf{k},c'}) \, P_{\mathbf{k},c'} \\ + \sum_{c} P_{\mathbf{k},c} \, v^{SIC\dagger}_{\mathbf{k},c} \, Q_{\mathbf{k}}. \end{aligned} \tag{28}$$

To fulfil the hermiticity of $h_{u,\mathbf{k}}$, the transformation matrix, M, and the localized states, ψ_n, have to be chosen so that the following quantity, named A_c, is real

$$\begin{aligned} A_c \; = \; \sum_{\mathbf{T},n} \int_{\Omega_{unit}} d\mathbf{r} \; \Psi^{*}_{\mathbf{k},c}(\mathbf{r}) \; M^{-1}_{c,n}(\mathbf{k}) \exp(-\mathrm{i}\mathbf{k}\mathbf{T}) w_n(\mathbf{r}+\mathbf{T}) \\ \psi_n(\mathbf{r}+\mathbf{T}). \end{aligned} \tag{29}$$

To show that Eqs. (25) and (16) are equivalent let the Hamiltonian $h_{u\mathbf{k}}$, as defined by Eq. (28), act on the SI corrected Bloch state, $\Psi_{\mathbf{k},c}$. This gives

$$\begin{aligned} (h^{\mathrm{LSD}} \; + \; v^{\mathrm{SIC}}_{\mathbf{k},c}) \, |\Psi_{\mathbf{k},c}\rangle \; = \; \varepsilon_{\mathbf{k},c} \, |\Psi_{\mathbf{k},c}\rangle \\ + \sum_{c';(c'\neq c)} \langle \Psi_{\mathbf{k},c'} | h^{\mathrm{LSD}} + v^{\mathrm{SIC}}_{\mathbf{k},c} | \Psi_{\mathbf{k},c}\rangle \, |\Psi_{\mathbf{k},c'}\rangle. \end{aligned} \tag{30}$$

Similarly, for the non-SI corrected state $\Psi_{\mathbf{k},nc}$ we get

$$h^{\mathrm{LSD}}\,|\Psi_{\mathbf{k},nc}\rangle \;=\; \varepsilon_{\mathbf{k},nc}\,|\Psi_{\mathbf{k},nc}\rangle \\ -\sum_{c}\langle\Psi_{\mathbf{k},c}|v^{SIC\dagger}_{\mathbf{k},c}|\Psi_{\mathbf{k},nc}\rangle\;|\Psi_{\mathbf{k},c}\rangle. \tag{31}$$

When interpreting the matrix elements on the right-hand side of Eqs. (30) and (31) as the elements of the Lagrange multipliers matrix, $\lambda_{\mathbf{k}}$, then Eqs. (30) and (31) are, indeed, equivalent to Eq. (16). The eigenvalues $\varepsilon_{\mathbf{k},\nu}$ are the diagonal elements of λ.

The transformation from real space to **k**-space, as defined by Eq. (14) and applied to Eq. (7), leads to the following localization criterion for the Bloch states

$$\int_{\Omega_{unit}} d\mathbf{r}\Psi^{*}_{\mathbf{k},\nu_1}\;(v^{SIC*}_{\mathbf{k},\nu_1}(\mathbf{r})\;-\;v^{\mathrm{SIC}}_{\mathbf{k},\nu_2}(\mathbf{r}))\;\Psi_{\mathbf{k},\nu_2}(\mathbf{r})\;=\;0. \tag{32}$$

Inspecting the r.h.s. of Eq. (30), containing the Lagrange multipliers of the subspace of the SI corrected Bloch states, one can see that the above equation guarantees the hermiticity of the corresponding subblock of $\lambda_{\mathbf{k}}$. Summarizing, the unified Hamiltonian approach is seen to yield both the orthogonalized SI corrected and non-SI corrected Bloch states, as well as the Lagrange multipliers matrix, all just from one matrix diagonalization per **k**-point.

The unified Hamiltonian scheme may readily be incorporated into the linear muffin-tin orbital (LMTO) band structure method,[17,35] and in what follows we shall describe the necessary steps in some detail.

The lattice Fourier transforms of the muffin tin orbitals (MTO's), $\chi_{\sigma,I,\mathbf{k}}(\mathbf{r})$, are used as a set of one-particle basis states. The label I stands for the angular momentum quantum numbers l, m and the site τ corresponding to the head of the MTO, while σ denotes the spin component. The space coordinate is decomposed as $\mathbf{r} = \boldsymbol{\rho} + \boldsymbol{\tau}$, with $\boldsymbol{\rho}$ restricted to the central unit cell. The Bloch states have the form

$$\Psi_{\sigma,\mathbf{k},\nu}(\boldsymbol{\rho},\tau)\;=\;\sum_{I}A^{(\nu)}_{\sigma,I;\mathbf{k}}\;\chi_{\sigma,I,\mathbf{k}}(\boldsymbol{\rho},\tau). \tag{33}$$

The wave vector coefficients, $\mathrm{A}^{(\nu)}_{\sigma,I;\mathbf{k}}$, and the one particle energies, $\varepsilon_{\sigma,\mathbf{k},\nu}$, are obtained by solving the following eigenvalue problem

$$\sum_{I'}\langle\chi_{\sigma,I,\mathbf{k}}|h_{u\mathbf{k}}|\chi_{\sigma,I',\mathbf{k}}\rangle\rangle\;A^{(\nu)}_{\sigma,I';\mathbf{k}} = \\ \varepsilon_{\sigma,\mathbf{k},\nu}\;\sum_{I'}\langle\chi_{\sigma,I,\mathbf{k}}|\chi_{\sigma,I',\mathbf{k}}\rangle\;A^{(\nu)}_{\sigma,I';\mathbf{k}}. \tag{34}$$

Making use of Eq. (27) leads to the following form of the matrix elements of the unified Hamiltonian

$$\begin{aligned}
&\langle\chi_{\sigma,I,\mathbf{k}}|h_{u\mathbf{k}}|\chi_{\sigma,I',\mathbf{k}}\rangle \;=\; \langle\chi_{\sigma,I,\mathbf{k}}|h^{\mathrm{LSD}}|\chi_{\sigma,I',\mathbf{k}}\rangle \\
&-\sum_{c,c',c\neq c'}\sum_{\nu}\langle\chi_{\sigma,I,\mathbf{k}}|\Psi_{\sigma,\mathbf{k},c}\rangle\langle\Psi_{\sigma,\mathbf{k},c}|\Psi^{\mathrm{LSD}}_{\sigma,\mathbf{k},\nu}\rangle \\
&\varepsilon^{\mathrm{LSD}}_{\sigma,\mathbf{k},\nu}\langle\Psi^{\mathrm{LSD}}_{\sigma,\mathbf{k},\nu}|\Psi_{\sigma,\mathbf{k},c'}\rangle\langle\Psi_{\sigma,\mathbf{k},c'}|\chi_{\sigma,I',\mathbf{k}}\rangle \\
&+\sum_{c}\langle\chi_{\sigma,I,\mathbf{k}}|\Psi_{\sigma,\mathbf{k},c}\rangle\langle\Psi_{\sigma,\mathbf{k},c}|v^{\mathrm{SIC}}_{\mathbf{k},c}|\Psi_{\sigma,\mathbf{k},c}\rangle\langle\Psi_{\sigma,\mathbf{k},c}|\chi_{\sigma,I',\mathbf{k}}\rangle \\
&+(\sum_{nc,c}\langle\chi_{\sigma,I,\mathbf{k}}|\Psi_{\sigma,\mathbf{k},nc}\rangle\langle\Psi_{\sigma,\mathbf{k},nc}|v^{\mathrm{SIC}}_{\mathbf{k},c}|\Psi_{\sigma,\mathbf{k},c}\rangle \\
&\langle\Psi_{\sigma,\mathbf{k},c}|\chi_{\sigma,I',\mathbf{k}}\rangle \;+\; c.c.\;). \qquad (35)
\end{aligned}$$

In the second term on the right-hand side of the above equation, we have inserted a complete set of the LSD Bloch states, $\Psi^{\mathrm{LSD}}_{\sigma,\mathbf{k},\nu}$, with the corresponding eigenvalues $\varepsilon^{\mathrm{LSD}}_{\sigma,\mathbf{k},\nu}$. Next, instead of using the MTO's, we can express all quantities in terms of the normalized single-site solutions, ϕ, and their energy derivatives, $\dot{\phi}$, at fixed energies $\varepsilon_{\sigma,l,\tau}$, and in the spherical potential V^{LSD}, and the magnetic field $\mathbf{B}^{\mathrm{LSD}}$. In the representation of these states $\Phi_{\sigma,I,1}(\boldsymbol{\rho}) = \phi_{\sigma,I}(\boldsymbol{\rho})$, and $\Phi_{\sigma,I,2}(\boldsymbol{\rho}) = \dot{\phi}_{\sigma,I}(\boldsymbol{\rho})$, the Bloch states read as

$$\Psi_{\sigma,\mathbf{k},\nu}(\boldsymbol{\rho},\tau) = \sum_{I,i} a^{(\nu)}_{\sigma,I,i;\mathbf{k}}\Phi_{\sigma,I,i}(\boldsymbol{\rho}). \qquad (36)$$

The relation between the coefficients $a^{(\nu)}_{\sigma,I,i;\mathbf{k}}$ on the one hand and the coefficients $A^{(\nu)}_{\sigma,I;\mathbf{k}}$ on the other, is provided by the standard LMTO formalism.[35] Similarly, the MTO's may be written in the form

$$\chi_{\sigma,I,\mathbf{k}}(\boldsymbol{\rho},\tau') = \sum_{I',i} \Gamma_{\sigma,I,I',i;\mathbf{k}}\Phi_{\sigma,I',i}(\boldsymbol{\rho}). \qquad (37)$$

Inserting Eq. (36) into Eq. (15) we obtain the corresponding representation of the localized states, ψ_n

$$\psi_n(\mathbf{r}+\mathbf{T}) = \psi_n(\boldsymbol{\rho},\tau;\mathbf{T}) \;=\; \sum_{l,m,i} C^{(n)}_{\sigma,I,i;\mathbf{T}}\Phi_{\sigma,I,i}(\boldsymbol{\rho}) \qquad (38)$$

with

$$C^{(n)}_{\sigma,I,i;\mathbf{T}} \;=\; \frac{1}{\Omega_{BZ}}\sum_{\nu}\int d\mathbf{k}\; M_{n,\nu}(\mathbf{k})\exp(\mathrm{i}\mathbf{k}\mathbf{T})a^{(\nu)}_{\sigma,I,i;\mathbf{k}}.$$

Making use of Eqs. (36) to (38) and (17), we can calculate the matrix elements of the unified Hamiltonian, $h_{u,\mathbf{k}}$, with

$$\begin{aligned}
\langle \chi_{\sigma,I,\mathbf{k}} | \Psi_{\sigma,\mathbf{k},\nu} \rangle &= \sum_{I',i} \Gamma_{\sigma,I,I',i;\mathbf{k}}\, a^{(\nu)}_{\sigma,I',i}\, g_{I',i} \\
\langle \Psi_{\sigma,\mathbf{k},\nu} | v^{\mathrm{SIC}}_{\mathbf{k},c} | \Psi_{\sigma,\mathbf{k},c} \rangle &= \sum_{n,\mathbf{T}} M^{-1}_{c,n}(\mathbf{k}) \exp(-\mathrm{i}\mathbf{k}\mathbf{T}) \sum_{I,i,i'} a^{(\nu)*}_{\sigma,I,i;\mathbf{k}} C^{(n)}_{\sigma,I,i',\mathbf{T}} \\
&\quad \times \int d\boldsymbol{\rho} \Phi^{*}_{\sigma,I,i}(\boldsymbol{\rho}) w^{SIC,av}_{n}(\rho,\tau;\mathbf{T}) \Phi_{\sigma,I,i'}(\boldsymbol{\rho}). \qquad (39)
\end{aligned}$$

Here $g_{I,i} = \langle \Phi_{I,i} | \Phi_{I,i} \rangle$, and we have approximated the SIC potential w^{SIC}_n by its spherical average, $w^{SIC,av}_n$, over the ASA sphere at site τ in the cell $\mathbf{T}$. Then it is also straightforward to express the energy functionals E^{LSD} and E^{SIC} in terms of quantities defined above.

As can be seen from Eq. (35), the SIC-LSD implementation is much more complicated than the LSD, because the Hamiltonian matrix elements depend explicitly on the Bloch states $\Psi_{\sigma,\mathbf{k},\nu}$. Consequently, one has to iterate the appropriate set of equations until the self-consistency for the one-particle potential, V^{LSD}, is achieved, and in addition, the unified Hamiltonian becomes consistent with its solutions. In practice, it turns out, that the self-consistency with respect to all necessary quantities, can be reached within a moderate number of iterations, if the Hamiltonian, $h^{(i)}_u$, for the i^{th} iteration is evaluated using the Bloch states of the previous iteration. In contrast, the transformation matrix, M, the localized states, ψ_n, and the SIC potentials, $v^{\mathrm{SIC}}_{\mathbf{k},\nu}$, are derived from the eigenstates of $h^{(i)}_u$. In the first iteration one starts with LSD Bloch states. The LSD potential, V^{LSD}, is obtained by mixing the total charge densities of previous iterations in the usual way. In practice, the evolution of the total energy, E_{tot}, is a suitable measure of the progress made in approaching overall self-consistency: If E_{tot} is converged to within $10^{-4} - 10^{-5}$ Ry, then also all other quantities turn out to be sufficiently well converged.

In contrast to the LSD, the SIC-LSD formalism gives a great deal of variational freedom to the DFT. At the beginning of each calculation one has to decide on the number and the character of the localized states ψ_n, e.g., their orbital moment- and spin-quantum numbers, and the sites to which they belong. This choice depends on the nature of the system in question and is guided by physical intuition. In general, it is not unique. We have the freedom to try different, but reasonable, 'configurations'. After carrying each of them to self-consistency the resulting total energies, E_{tot}, are compared, and the configuration corresponding to the lowest total energy is considered to provide the best description of the physical situation, as described within the SIC-LSD scheme. Of course, there always exists a possibilty that the LSD will provide the minimum of E_{tot}, meaning that the SI corrections are of no importance for the system in question.

4 The Steepest Descent Approach

An alternative way to solve the SIC-LSD equations, Eq. (6), is by the steepest descent method,[20] whereby the $E^{\text{SIC-LSD}}$ functional is minimized iteratively. If at some point approximative solutions $\tilde{\psi_\alpha}$ are given, the energy may be further minimized by adding a correction proportional to the gradient of $E^{\text{SIC-LSD}}$. Specifically,

$$\tilde{\psi_\alpha} \to \tilde{\psi_\alpha} + \delta\psi_\alpha, \tag{40}$$

with

$$\delta\psi_\alpha(\mathbf{r}) = -x\ \hat{Q}\ \frac{\delta E^{\text{SIC-LSD}}}{\delta\psi^*_\alpha(\mathbf{r})}, \tag{41}$$

where $\hat{Q}$ projects onto the space orthogonal to the occupied states:

$$\hat{Q} = 1 - \sum_{\alpha}^{occ.} |\tilde{\psi_\alpha}\rangle\langle\tilde{\psi_\alpha}|. \tag{42}$$

The gradient in Eq. (41) is given by the SIC Hamiltonian in Eq. (6), so that

$$\delta\psi_\alpha = -x \left[(h^{\text{LSD}} + w^{\text{SIC}}_\alpha)\tilde{\psi_\alpha} - \sum_\beta \lambda_{\alpha,\beta}\ \tilde{\psi_\beta} \right]. \tag{43}$$

The localization criterion, Eq. (7), may be fulfilled by adding to $\tilde{\psi_\alpha}$ a correction term given by

$$\delta\psi_\alpha = -y \sum_\beta r_{\alpha,\beta}\ \tilde{\psi_\beta} \tag{44}$$

$$r_{\alpha,\beta} = \lambda_{\alpha,\beta} - \lambda^*_{\beta,\alpha}, \tag{45}$$

while a third type of correction term is needed to keep the orbitals ψ_α orthonormal:

$$\delta\psi_\alpha = -\frac{1}{2} \sum_\beta t_{\alpha,\beta}\ \tilde{\psi_\beta}, \tag{46}$$

with

$$t_{\alpha,\beta} = \langle\tilde{\psi_\alpha}|\tilde{\psi_\beta}\rangle - \delta_{\alpha,\beta}. \tag{47}$$

The steps (43), (44) and (46) may be interchanged and the parameters x and y chosen according to the problem at hand. At convergence all steps vanish, and it is seen that a vanishing step in Eq. (43) corresponds to Eq. (6), a vanishing step (44) corresponds to Eq. (7), and a vanishing step (46) corresponds to orthonormality, $t_{\alpha,\beta} = 0$.

When the one-electron wavefunctions are expanded in a basis set, χ_i, as

$$\psi_\alpha = \sum_i a_i^\alpha \, \chi_i \,, \tag{48}$$

where i is a composite index labelling the degrees of freedom of the basis, the steps (43), (44) and (46) are turned into matrix operations on the vector a of expansion coefficients. In our actual implementation, the χ_i's are conveniently chosen as TB-LMTO functions.[21] in which case i labels atomic sites and angular momentum and spin quantum numbers, as discussed in connection with Eq. (33). The steps then read

$$\delta a^\alpha = -x \, (\mathbf{O}^{-1} - \mathit{\Pi}) \cdot (\mathbf{H} + \mathbf{V}^\alpha) \cdot a^\alpha \,, \tag{49}$$

$$\delta a^\alpha = -y \sum_\beta r_{\alpha,\beta} \, a^\beta \,, \tag{50}$$

$$\delta a^\alpha = \frac{1}{2} \, (\mathbf{O}^{-1} - \mathit{\Pi}) \cdot \mathbf{O} \cdot a^\alpha \,, \tag{51}$$

respectively. Here, $\mathbf{O}$, $\mathbf{H}$ and $\mathbf{V}^\alpha$ are the overlap, the Hamiltonian, and the SIC-potential matrices:

$$\mathbf{O}_{ij} = \langle \chi_i | \chi_j \rangle, \tag{52}$$

$$\mathbf{H}_{ij} = \langle \chi_i | h^{\mathrm{LSD}} | \chi_j \rangle, \tag{53}$$

$$\mathbf{V}^\alpha_{ij} = \langle \chi_i | w^{\mathrm{SIC}}_\alpha | \chi_j \rangle. \tag{54}$$

and $\mathit{\Pi}$ is given by

$$\mathit{\Pi}_{ij} = \sum_\beta^{occ.} \delta_{\sigma_\alpha \sigma_\beta} \cdot a_i^{\beta *} \, a_j^\beta, \tag{55}$$

where the δ-function ensures that only projection on states with the same spin as ψ_α is considered. In a periodic lattice, $\mathbf{O}$, $\mathbf{H}$, and $\mathit{\Pi}$ are translational invariant. For $\mathit{\Pi}$ this follows from the translational invariance (8), which for the expansion coefficients means that (setting $\alpha \equiv (n, \mathbf{T})$, with $\mathbf{T}$ a lattice translation):

$$a^{n,\mathbf{T}}_{(\boldsymbol{\tau}+\mathbf{R})L} = a^{n,\mathbf{0}}_{(\boldsymbol{\tau}+\mathbf{R}-\mathbf{T})L} \cdot \tag{56}$$

Here L enumerates the angular momentum characteristics of the TB-LMTO function. Only the SIC potential matrix $\mathbf{V}^\alpha$ is not translational invariant, and requires special attention. As in the unified Hamiltonian approach the translational invariance is exploited by switching to $\mathbf{k}$-space: We assume $\mathbf{R}$ running over a finite cluster (M unit cells with periodic boundary clusters, where M must be so large as to ensure that the SIC states vanish outside this region). Let $\mathbf{k}$ enumerate the corresponding reciprocal space, i. e., the $M \times M$ matrix $\mathbf{U}_{\mathbf{kR}} \equiv \frac{1}{\sqrt{M}} e^{\mathrm{i}\mathbf{k}\cdot\mathbf{R}}$ is unitary: $\mathbf{U}\mathbf{U}^+ = \mathbf{U}^+\mathbf{U} = \mathbf{1}$. Then Eqs. (49)-(51) hold for the Fourier transformed quantities as well, except for the product $\mathbf{V}^\alpha a^\alpha$, which must

first be evaluated in real space and Fourier transformed afterwards. Specifically, let

$$b^{n,\mathbf{T}}_{(\boldsymbol{\tau}+\mathbf{R})L} = \langle \chi_{(\boldsymbol{\tau}+\mathbf{R})L} | V^{\mathrm{SIC}}_{n,\mathbf{T}} | \psi_{n,\mathbf{T}} \rangle \,. \tag{57}$$

Then, with

$$b^{n}_{\boldsymbol{\tau}L}(\mathbf{k}) = \frac{1}{\sqrt{M}} \sum_{\mathbf{R}} e^{\mathrm{i}\mathbf{k}\cdot(\mathbf{R}-\mathbf{T})}\, b^{n,\mathbf{T}}_{(\boldsymbol{\tau}+\mathbf{R})L} \,, \tag{58}$$

we get

$$\delta a^n(\mathbf{k}) = -x\,(\mathbf{O}^{-1}(\mathbf{k}) - \mathit{\Pi}(\mathbf{k})) \cdot [\mathbf{H}(\mathbf{k}) \cdot a^n(\mathbf{k}) + b^n(\mathbf{k})] \,, \tag{59}$$

$$\delta a^n(\mathbf{k}) = -y \sum_{n'} r_{n,n'}(\mathbf{k})\, a^{n'}(\mathbf{k}) \,, \tag{60}$$

and

$$\delta a^\nu(\mathbf{k}) = \frac{1}{2}\,(\mathbf{O}^{-1} - \mathit{\Pi}) \cdot \mathbf{O} \cdot a^\nu \tag{61}$$

for the gradient-step, the unitarian-mixing step and the orthonormalizing step, respectively. The r-matrix in $\mathbf{k}$-space in (60) is simply given by:

$$r_{n,n'}(\mathbf{k}) = \sum_{\boldsymbol{\tau}L} [a^{n'*}_{\boldsymbol{\tau}L}(\mathbf{k}) \cdot b^{n}_{\boldsymbol{\tau}L}(\mathbf{k}) - b^{n'*}_{\boldsymbol{\tau}L}(\mathbf{k}) \cdot a^{n}_{\boldsymbol{\tau}L}(\mathbf{k})] \,. \tag{62}$$

5 The Relativistic Extension

For many applications it is desirable to take account of all relativistic effects, including the spin-orbit coupling. This is not only important when we are concerned with systems containing heavy atoms, but also if we, e.g., intend to get reasonable results for properties depending on orbital moments and their coupling to the spins of the electrons. Furthermore, the localized states resulting from the SI corrections are especially sensitive to the relativistic effects. Therefore, we generalize the SIC-LSD formalism, described in the previous section, to a fully relativistic spin-polarized case. The steps involved are in close analogy to the derivation of the relativistic LSD-LMTO method by Ebert [22].

The LSD wave equation of the scalar relativistic theory, where the two spin channels, as well as the orbital- and spin-moments are decoupled, is now replaced by the Dirac equation.[23] The relativistic generalization of Eq. (3) reads as

$$h^{\text{LSD-REL}} = (\hat{T}^{\mathrm{REL}} \;+\; V^{\mathrm{LSD}} + \beta\boldsymbol{\sigma} \cdot \mathbf{B}^{\mathrm{LSD}}(\mathbf{r}))\psi_\alpha(\mathbf{r}) \;=\; \varepsilon_\alpha \psi_\alpha(\mathbf{r}) \tag{63}$$

with

$$\hat{T}^{\mathrm{REL}} \;=\; \boldsymbol{\alpha}\, \frac{1}{i}\nabla + \frac{1}{2}(\beta - I). \tag{64}$$

Here $\boldsymbol{\alpha}, \beta$ are the Dirac matrices, while I is the unit matrix. The wave functions ψ_α, specifically their kets, are now four-component column vectors, wheras their bras are the row-vectors with complex conjugate elements.

The equations (1) to (32) remain valid in the relativistic case provided one replaces the operators $\boldsymbol{\sigma}$ and $\hat{T}$ with the matrices $\beta\boldsymbol{\sigma}$ and $\hat{T}^{\mathrm{REL}}$, respectively [23]. The other operators should be interpreted as diagonal matrices. The main complication arises from the nature of the single-site wave functions of the Hamiltonian $h^{\text{LSD-REL}}$. They are to a good approximation simultaneously the eigenfunctions of the orbital moment, l, and the z-component, μ, of the total angular momentum, $\mathbf{j}$. In the case of $|\mu| < l+1/2$ there exist two independent solutions for these quantum numbers ($is = 1, 2$), and each solution is the sum of two components (ic=1,2), having total angular momentum $j_{ic=1} = l + 1/2$ and $j_{ic=2} = l - 1/2$, respectively. In the case of $|\mu| = l + 1/2$, on the other hand, there is only one solution which in addition is an eigenfunction of the total angular momentum $j = l + 1/2$. The relativistic generalization of the single-site wave functions, Φ_{σ,I,i_1}, of the scalar relativistic theory, as introduced in Eq. (36), become

$$\Phi^{(\kappa)}_{I,is,i}(\boldsymbol{\rho}) = \Phi^{(\kappa)}_{I,1,is,i}(\boldsymbol{\rho}) + (1 - \delta_{|\mu|,l+1/2})\, \Phi^{(\kappa)}_{I,2,is,i}(\boldsymbol{\rho}) \tag{65}$$

with

$$\Phi^{(\kappa)}_{I,ic,is,i}(\boldsymbol{\rho}) = R^{(\kappa)}_{I,ic,is,i}(\rho)\mathbf{Y}_{j_{ic},\mu,l_{ic,\kappa}}(\boldsymbol{\rho}). \tag{66}$$

Here $R^{(\kappa)}_{I,ic,is,i}$ is the radial part of the ic component of the single-site solution is, and the index I comprises the indices l, μ, as well as, the site-index τ. The $\kappa = 1$ corresponds to the large component and $\kappa = 2$ to the small component of the bispinor $\Phi_{I,ic,is,i}$. Then $l_{ic,\kappa}$ takes the values $l_{1,1} = l_{2,2} = l$, $l_{1,2} = l + 1$, and $l_{2,1} = l - 1$. The spinor functions $\mathbf{Y}_{j,\mu,l}$, are combinations of the spherical harmonics, $Y_{l,m}$, the spin functions, χ_s, and the Clebsch-Gordon-coefficients of the well known form

$$\mathbf{Y}_{j,\mu,l}(\boldsymbol{\rho}) = \sum_s < j, \mu | l, \mu - s, 1/2, s \rangle Y_{l,\mu-s}(\boldsymbol{\rho})\chi_s.$$

The matching of these single-site functions to the interstitial LMTO envelope functions, and the construction of the relativistic MTO's has been described by Ebert[22] and will not be repeated here. With the information given above, it is easy to see that Eqs. (33) to (39) apply to the relativistic case as well, provided the subscript σ is omitted, and the index $I(l, m, \tau)$ gets replaced by the indices $(I(l, \mu, \tau), is)$. Furthermore, an evaluation of the occuring quantities implies matrix- and vector-operations in spinor space. Since the dimension of the eigenvalue problem is doubled in comparison to the scalar relativistic case, it is obvious that fully relativistic calculations will be considerably more expensive. In addition, the computation of the matrix elements, especially those introduced by the SIC terms, is rather tedious and requires careful programming. As an

illustration, we conclude this section by displaying the relativistic version of Eq. (39), namely

$$\langle \Psi_{\mathbf{k},\nu} | v^{\mathrm{SIC}}_{\mathbf{k},c} | \Psi_{\mathbf{k},c} \rangle = \sum_{n,j} M^{-1}_{c,n}(\mathbf{k}) \exp(-\mathrm{i}\mathbf{k}\mathbf{T})$$
$$\sum_{I,i,i'} \sum_{\kappa,is,is'} a^{(\nu)*}_{I,is,i;\mathbf{k}} C^{(n)}_{I,is',i'} \langle \Phi^{(\kappa)}_{I,is,i} | w^{SIC,av}_n | \Phi^{(\kappa)}_{I,is',i'} \rangle_{\mathbf{T}} \tag{67}$$

with

$$\langle \langle \Phi^{\kappa}_{I,is,i} | w^{SIC,av}_n | \Phi^{\kappa}_{I,is',i'} \rangle_{\mathbf{T}} = \int \rho^2 d\rho \; v^{SIC,av}_n(\rho,\tau;\mathbf{T}) \sum_{ic} R^{(\kappa)}_{I,ic,is,i}(\rho)$$
$$R^{(\kappa)}_{I,ic,is',i'}(\rho) + \sum_{ic,ic'} Q(j_{ic}, j_{ic'}, \mu, l) \int \rho^2 d\rho \; b^{SIC,av}_n(\rho,\tau;\mathbf{T}) R^{(1)}_{I,ic,is,i}(\rho)$$
$$R^{(1)}_{I,ic',is',i'}(\rho) - \sum_{ic} Q(j_{ic}, j_{ic}, \mu, l_{2,ic}) \int \rho^2 d\rho \; b^{SIC,av}_n(\rho,\tau;\mathbf{T}) R^{(2)}_{I,ic,is,i}(\rho)$$
$$R^{(2)}_{I,ic,is',i'}(\rho)) \tag{68}$$

and

$$Q(j_1, j_2, \mu, l) = \sum_{s=(-1/2,1/2)} 2s < j_1 \mu | l, \mu - s, 1/2, s \rangle$$
$$\langle j_2 \mu | l, \mu - s, 1/2, s \rangle. \tag{69}$$

6 Applications

In this section we concentrate on results obtained within SIC-LSD for NiO, cerium metal and cerium monopnictides. For all these systems LSD fails in describing the correct physics. In NiO, as mentioned earlier, LSD underestimates the magnetic moment and leads to a vanishing band gap due to an inadequate treatment of the on-site Coulomb repulsion among $3d$ electrons. In solids containing cerium it is the f electrons that are not correctly represented within LSD, and the attention here is turned to a variety of structural and magnetic phase transitions, beyond the reach of LSD.

6.1 NiO

The calculated key parameters of NiO as given by LSD, LDA+U, SIC-LSD and Hartree-Fock theory are quoted in Table 1 and displayed in Fig. 1. Applying SIC-LSD to NiO is seen to lead to a substantial band gap of 3.15 eV, at the experimental volume, which compares reasonably well with the experimental value of about 4.2 eV [27]. Also the magnetic moment is improved with respect

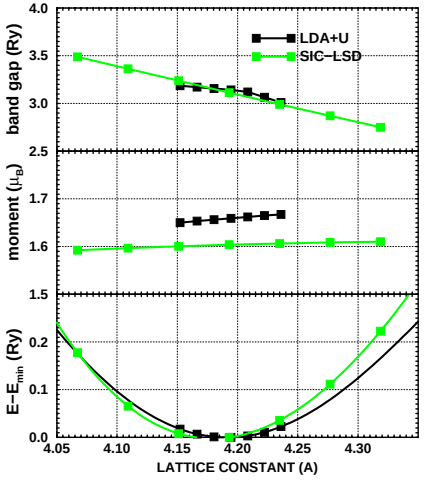

Fig. 1. The band gap, magnetic moment and the total energy of NiO in the antiferromagnetic unit cell as a function of the lattice constant, as calculated by LDA+U and SIC-LSD.

to the LSD result, and the lattice parameter is nearly spot on. The experimental values of the magnetic moment fall between 1.66 and 1.90 μ_B [8]. That SIC-LSD provides better treatment for the $3d$ electrons in this system is also supported by comparison with the results of LDA+U calculations [24], performed within the spin polarised generalisation of the method. The latter is yet another scheme that takes the on-site Coulomb repulsion, U, explicitly into account, however, U is often treated as a parameter and chosen such that some quantity agrees with its experimental value. In Fig. 1 we show the results of both schemes for the band gap, spin magnetic moment, and total energies, as functions of the lattice constant. The numerical values calculated by LDA+U and SIC-LSD agree well both between themselves and with the experimental data. It is interesting to note that according to both the LDA+U and SIC-LSD calculations the band gap in NiO increases with increasing pressure. The band gap was found to behave similarly in LSD. The value of the band gap is sensitive to the degree of charge transfer from Ni to O. If this charge transfer increases, the band gap decreases, because the unoccupied Ni d states move down in energy, while the occupied O p states move up in energy. We conclude that the SIC is the mechanism for producing a sizeable band gap in NiO, but the actual value of the gap reflects the charge transfer in the system.

In Table 1 we compare the SIC-LSD results for the band gap, lattice parameter and bulk modulus with the experimental results and those from other

Table 1. Parameters characterizing the electronic structure of crystalline NiO and its structural stability, as calculated by LSD, LDA+U (with a $\bar{U}$=6.2 eV) and SIC-LSD [24]. The Hartree-Fock (H-F) values and experimental data for NiO were taken from Towler et al. [25].

Quantity/Method	LSD	LDA+U	SIC-LSD	H-F	Experiment
lattice constant (**r**A)	4.08	4.19	4.18	4.26	4.17
band gap (eV)	0.5	3.0	3.15	14.2	4.2
$B = (C_{11} + 2C_{12})/3$ (GPa)	230, 236[a]	182	220	214	145, 205, 189

a : Ref. [26] .

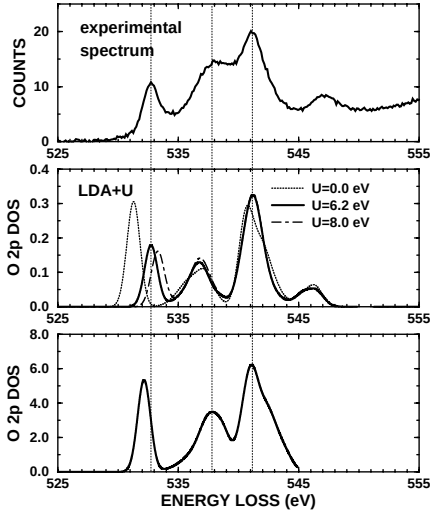

Fig. 2. Comparison of the experimental electron energy loss oxygen K edge spectrum of NiO with the density of empty oxygen $2p$ states of NiO, as calculated by LSD ($\bar{U} = 0$), LDA+U ($\bar{U} = 6.2$ and 8 eV), and SIC-LSD.

calculations within LDA+U, LSD and Hartree-Fock method. Note that, unlike in case of the SIC-LSD, the results for LSD and LDA+U refer to the full potential implementation of the LMTO method. The effect of the full potential can be seen in the LDA+U total energy curve in Fig. 1, at higher values of the lattice parameter, as compared with the one due to SIC-LSD. This, however, has not affected the minima of the respective curves, as can be seen from Table 1.

A further demonstration of the advantages of SIC-LSD over LSD is presented in Fig. 2, where we compare the K edge EELS spectra of NiO with the

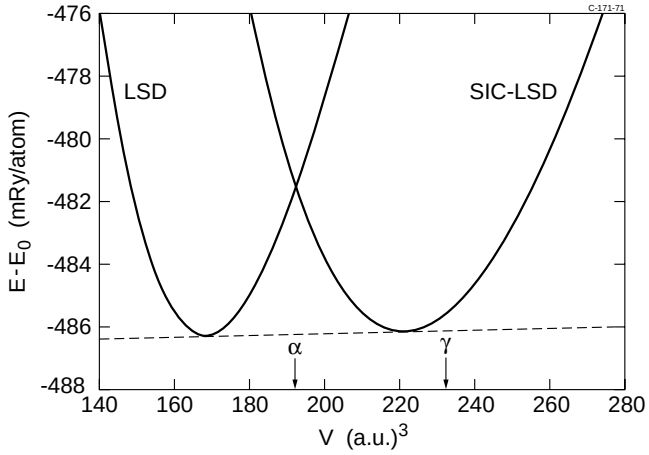

Fig. 3. Cohesive energy of Ce (in mRy/atom) as a function of atomic volume (in a_0^3/atom). The curve marked 'SIC-LSD' corresponds to the calculation with one localized $f-$electron per Ce atom, while the curve marked 'LSD' corresponds to itinerant $f-$electrons. The common tangent marks the phase transition.

calculations performed within LSD, LDA+U and SIC-LSD. The structure of the experimental EELS spectrum shown in Fig. 2 is dominated by the the dipole {filled 1s}→{empty 2p} transitions. Figure 2 shows that the unoccupied O 2*p* density of states (DOS) calculated using LSD does not agree well with the experimental EELS spectrum. The peaks in the EELS spectrum are associated with the hybridization between oxygen 2*p* and nickel 3*d*, 4*s* and 4*p* states, respectively, and our analysis shows that the latter two peaks are practically unaffected by Hubbard correlations in the 3*d* shell. The separation between the two main peaks, namely, the O 2*p*-Ni 3*d* and O 2*p*-Ni 4*p* peaks, as seen in the LSD DOS curve, is approximately 2 eV larger than the separation between the same peaks in the experimental spectrum, and the spectral weight of the low-energy peak in the DOS calculated using LSD is far too high. Performing the LDA+U calculation for the O 2*p* DOS, with U=6.2 eV, leads to a significant improvement over LSD. Considering SIC-LSD result, that unlike LDA+U does not contain any adjustable parameters, the agreement with experiment is rather good. The SIC-LSD O 2*p* DOS shows slightly reduced separation between the two main peaks in the spectrum, and thus improves the agreement with the experimental EELS spectra, as compared to LSD.

6.2 Cerium

As mentioned in the introduction, LSD was not able to explain the $\gamma \rightarrow \alpha$ phase transition in cerium although it gave a magnetic solution for the lattice parameter close to the experimental value of $\gamma-$Ce. The SIC-LSD, however, provides a unified description of this transition with the total quenching of the magnetic moment and volume collapse of 24 %. The calculated transition pressure of -1

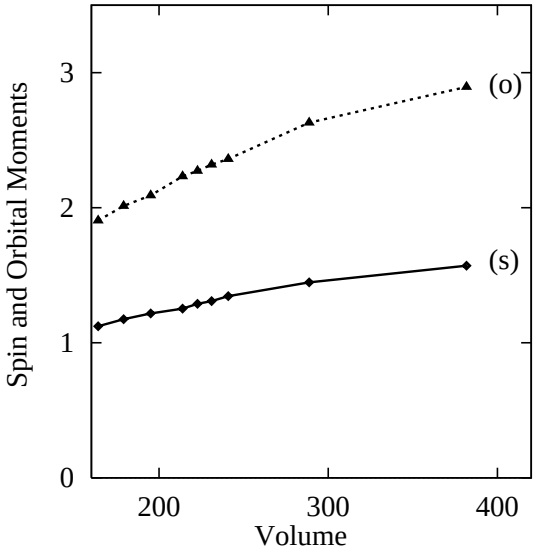

Fig. 4. Spin (s) (in μ_B) and orbital (o) moments as a function of volume (in (a.u.)^3) within the relativistic SIC-LSD approximation in $\gamma-$Ce.

kbar compared favourably with the value of -7 kbar, extrapolated from the experimental phase diagram to T=0K, at which the calculations were performed. The volume collapse associated with the transition is shown in Fig. 3, where the calculated total energy of Ce as a function of volume is shown [28–30]. The two different curves correspond, respectively, to the $\alpha-$phase (curve marked LSD; SIC–LSD reduces to the LSD for delocalized electrons) and $\gamma-$phase (curve marked SIC–LSD). The LSD minimum of the total energy, corresponding to the $\alpha-$phase, is located in the non–magnetic region at V = 168 (a.u.)^3, while the spin magnetic moment is m = $1.32\mu_B$ at the SIC–LSD total energy minimum, corresponding to the $\gamma-$phase. Within these *ab initio* calculations, the $\gamma\rightarrow\alpha$ transition can be viewed as the transition between the phase with fully localized f electrons and the phase, where the f electrons are fully delocalized.

Performing the fully relativistic SIC-LSD calculations allows one to study also the orbital moment of the γ–phase of Ce [31]. In Fig. 4 the orbital moment can be seen to extrapolate to the atomic value of 3 at large volumes. This is the localization of one f electron within the relativistic SIC-LSD theory that suffices to describe the substantial spin and orbital moments in $\gamma-$Ce. The relativistic SIC-LSD scheme allows for each of the 14 possible $f-$states in Ce to become localized. As seen in Table 2, one finds that these 14 possible solutions have quite different orbital moments and correspond to different total energies. The 14 solutions have the block structure of 2+6+6. The ground state solution has

the characteristics of a good crystal field-like state: sizeable spin and orbital moments which are anti-parallel aligned. The other solutions are substantially different from what one would expect from crystal field considerations. We find 6 solutions with energies 9.4 mRy higher than the lowest energy solution. These solutions are characterized by an orbital moment which is over 4 times smaller than the one of the ground state, but a spin moment substantially unaltered. Finally we have 6 solutions, situated 6.3 to 7.9 mRy above the minimum, whose orbital moment is essentially zero and whose spin moment is smaller than that of the other solutions. The total energy differences in Table 2 could be interpreted as excitation energies to populate each of the 14 localized states, corresponding to different spatial symmetry. We note that the solutions fulfill time-reversal symmetry: 7 spin ups and 7 spin downs, nearly all pairwise equal. The small deviations from exact spin up and down symmetry should be considered as the measure of the accuracy of our calculations. In Table 2 we also present the contributions to the spin and orbital moments due to the SIC localized states only, M_s^{loc} and L_z^{loc}, respectively. Regarding the total orbital moment, one can see that nearly the whole contribution comes from the localized state, whilst in case of the total spin moment 74% comes from the localized state, and the delocalized states contribute the remaining 26%.

Table 2. Calculated total energy differences with respect to the ground state (in mRy), orbital and magnetic (in μ_B) moments of the $\gamma-$phase of Ce. Also quoted are the local orbital and magnetic moments of the localized state.

M_s	$M_s{}^{loc}$	L_z	$L_z{}^{loc}$	ΔE
1.310	0.960	−2.290	−2.240	0.0
−1.309	−0.966	2.317	2.305	0.0
1.259	0.923	−0.053	0.034	6.3
1.275	0.935	−0.060	0.028	6.7
−1.257	−0.896	0.054	−0.032	6.9
−1.266	−0.913	0.021	−0.131	7.0
1.271	0.913	−0.024	0.128	7.9
−1.271	−0.912	0.032	−0.120	7.9
1.293	0.986	−0.536	−0.432	9.4
−1.293	−0.985	0.536	0.432	9.4
1.293	0.985	−0.532	−0.429	9.4
−1.293	−0.985	0.532	0.429	9.4
1.293	0.985	−0.510	−0.408	9.4
−1.293	−0.985	0.535	0.432	9.4

The solution with the lowest total energy is consistent with all three Hund's Rules, and the spin and orbital moments are anti-parallel aligned. This gives one confidence that the relativistic SIC–LSD scheme forms a bridge between the atomic and band pictures, and enables one to obtain a good description of

both the localized and itinerant properties of a rare earth metal. The SIC-LSD relativistic band theory preserves all characteristic features of the $\gamma \rightarrow \alpha$ transition in Ce, and explains it as a transition from a localized state with maximum spin and orbital moments to a delocalized state without spin and orbital moments.

Table 3. Calculated transition pressures for the electronic and structural phase transitions in the cerium pnictides. Also quoted are the specific volumes on the two sides of the transition [32] . The notation (d) and (l) refers to calculations with delocalized or localized Ce $f-$electrons, i.e. tetravalent or trivalent Ce atoms. B2* denotes a slightly distorted B2 structure (see Ref. [39] for discussion).

compound	transition	P_t (kbar)		V_h ($a_0{}^3$)		V_l ($a_0{}^3$)	
		theo.	expt.	theo.	expt.	theo	expt.
CeN	B1(d) $\rightarrow$ B2(d)	620	-	148	-	141	-
CeP	B1(l) $\rightarrow$ B1(d)	71	90[a],55[b]	325	308[a]	297	2 98[a]
CeP	B1(d) $\rightarrow$ B2(d)	113	150(40)[a]	288	285[a]	246	247[a]
CeAs	B1(l) $\rightarrow$ B2(d)	114	140(20)[c]	332	315[c]	265	274[c]
CeSb	B1(l) $\rightarrow$ B2*(l)	70	85(25)[d]	400	398[d]	353	354[d]
CeSb	B2*(l) $\rightarrow$ B2*(d)	252	-	311	-	295	-
CeBi	B1(l) $\rightarrow$ B2*(l)	88	90(40)[e]	427	399[e]	376	360[e]
CeBi	B2*(l) $\rightarrow$ B2*(d)	370	-	317	-	304	-

a: Ref. [33]. b: Ref. [34].
c: Ref. [35]. d: Ref. [36] .
e: Ref. [37] .

6.3 Cerium Monopnictides

The cerium monopnictides, CeN, CeP, CeAs, CeSb and CeBi, undergo a variety of structural and magnetic phase transitions under pressure. They have been thoroughly studied experimentally, and here we discuss a comparison of those studies with the SIC-LSD calculations. A detailed summary of our SIC-LSD calculations is given in Table 3, where we present the respective transition pressures and volumes associated with a variety of transitions in comparison with the experimental data. The SIC-LSD calculations involved the total energy calculations as a function of volume for CeN, CeP, CeAs, CeSb and CeBi for B1 and B2 structural phases, in the ferromagnetic (F) arrangement of Ce moments, and with the $f-$electron treated as either delocalized (LSD) or localized (SIC-LSD) [38,39,30].

As can be seen in Table 3, the calculations faithfully reproduce the pressure behaviour of the Ce pnictides. In particular, we find that only for CeN the f electron is delocalized at ambient conditions, while the other cerium pnictides are characterized by localized f electrons, in accordance with experimental observation. For CeP two phase transitions are observed, first the delocalization transition and subsequently the structural transition from B1 to B2 structure.

The two transitions merge into a single one for CeAs, namely a transition from a B1 structure with the f electron localized to a B2 structure with the f electron delocalized. For the two remaining systems, CeSb and CeBi, the structural transition occurs first and at higher pressures does the f electron become delocalized. This trend may be understood in terms of increasing f electron localization with increasing nuclear charge of the ligand. Moreover, for CeSb and CeBi the SIC-LSD predicts a second isostructural B2→B2 transition to occur at higher pressures, where the $f-$electrons are delocalizing. It seems necessary to perform measurements for these systems at pressures above 250 kbar to clarify whether such transitions occur in reality.

The magnetic properties of cerium monopnictides, with the exception of CeN, are rather complicated with several antiferromagnetically ordered phases, including a Devil's staircase, and phase transitions as a function of pressure, temperature and applied magnetic field [34,40–43]. Therefore, we have for CeP performed a series of calculations exploring the energetics of various conceivable magnetic orderings. Apart from the ferromagnetic structure, LSD (delocalized f electrons) and SIC-LSD (localized f electrons) calculations were done in the AF1 and AF2 structures. In the AF1 structure the cerium moments are ferromagnetically ordered within (100) planes, which then are antiferromagnetically stacked in the (100) direction. Similarly, in the AF2 structure the cerium moments are ferromagnetically ordered within (111) planes, which are antiferromagnetically stacked in the (111) direction. In accordance with experiment an AF1 groundstate with the localized f electron [39] was obtained. The equilibrium volumes of the three magnetic structures were found to be virtually identical. CeP was found to be semimetallic in the minimum energy position in both the AF1 and AF2 structures, but at negative pressures (expanded volume), a semimetal-semiconductor transition took place. This semimetallic behaviour was found to originate from small hole pockets around the Γ point in the center of the Brillouin zone and compensated by electron pockets around the M point on the Brillouin zone boundary. These pockets are mostly confined to the basal plane of the Brillouin zone. These results are in agreement with de Haas-van Alphen [44,45] and photoemission [46] findings regarding the location of the electron and hole pockets.

7 Conclusions

We have described the SIC-LSD formalism that provides a mechanism for treating the static Coulomb correlations within *ab initio* band theory. We have demonstrated that it can treat both localized and delocalized electrons on equal footing, and owing to that is capable to study systems and properties for which LSD fails. What SIC-LSD does is to assign an energy contribution, the self-interaction correction, for an electron state to localize. Whether a system is localized or delocalized is then a result of a fight between this explicit 'localization energy' and the band formation energy. Both LSD and SIC-LSD are local minima of the DFT energy functional. Like LSD, SIC-LSD is still a one-electron theory and both work only in extreme situations. Namely, when $U/t \ll 1$, with

t being a typical hopping integral, LSD provides the correct physics, while for $U/t \gg 1$, SIC-LSD gives the valid description of the physical situation. Most importantly, as discussed in the present paper, SIC-LSD provides a correct description of pressure induced transitions from predominantly localized to predominantly delocalized groundstates, and is in general much more appropriate approach for systems with strong Coulomb correlation.

Acknowledgements This work has benefited from collaborations within, and has been partially funded by, the Training and Mobility Network on "Electronic structure calculations of materials properties and processes for industry and basic sciences" (Contract FMRX-CT98-0178).

References

1. P. Hohenberg and W. Kohn, Phys. Rev. **136**, B864 (1964): W. Kohn and L. J. Sham, Phys. Rev. A **140**, 1133 (1965).
2. R. O. Jones and O. Gunnarsson, Rev. Mod. Phys. **61**, 689 (1989).
3. W. Pickett, Rev. Mod. Phys. **61**, 433 (1989).
4. N. F. Mott, "Metal-Insulator Transitions" (Taylor and Francis, London, 1974).
5. B. Brandow, Adv. Phys. **26**, 651 (1977); J. Alloys and Compounds, **181**, 377 (1992).
6. K. Terakura, A. R. Williams, T. Oguchi and J. Kübler, Phys. Rev. Lett. **52**, 1830 (1984) ; Phys. Rev. B**30**, 4734 (1984).
7. J. Zaanen, G. A. Sawatzky and J. W. Allen, Phys. Rev. Lett. **55**, 418 (1985).
8. V. I. Anisimov, J. Zaanen and O. K. Andersen, Phys. Rev. B **44**, 943 (1991).
9. B. Johansson, Phil. Mag. **30**, 469 (1974).
10. J. W. Allen and R. M. Martin, Phys. Rev. Lett. **49**, 1106 (1982); J. W. Allen and L. Z. Liu, Phys. Rev. B **46**, 5047 (1992).
11. D. Glötzel, J. Phys. F **8**, L163 (1978); D. Glötzel and R. Podloucky, Physica **102B**, 348 (1980).
12. H. L. Skriver, O. K. Andersen and B. Johansson, Phys. Rev. Lett. **44**, 1230 (1980).
13. J. Hubbard, Proc. R. Soc. London A**276**, 238 (1963); A**277**, 237 (1964); A**281** 401 (1964)
14. V. I. Anisimov, F. Aryasetiawan and A. I. Liechtenstein, J. Phys.: Condens. Matter, **9**, 767 (1997).
15. J. P. Perdew and A. Zunger, Phys. Rev. B **23**, 5048 (1981); A. Svane, Phys. Rev. **B51**, 7924 (1995).
16. J. Taylor, "Scattering Theory", (Wiley, New York, 1972).
17. O. K. Andersen, Phys. Rev. B **12**, 3060 (1975);
18. J. G. Harrison, R. A. Heaton and C. C. Lin, J. Phys. B **16**, 2079 (1983).
19. H. L. Skriver, "The LMTO Method" (Springer Verlag, Berlin, 1984).
20. A. Svane, Phys. Rev. **B53**, 4275 (1996).
21. O. K. Andersen, O. Jepsen and O. Glötzel, "Canonical description of the band structures of metals", *in* Proc. of Int. School of Physics, Course LXXXIX, Varenna, 1985, ed. by F. Bassani, F. Fumi and M. P. Tosi (North– Holland, Amsterdam, 1985), p. 59.
22. H. Ebert, Phys. Rev. B**38**, 9390 (1988).

23. For a discussion of relativistic DFT, see P. Strange, *Relativistic Quantum Mechanics*, (Cambridge, 1998).
24. S.L. Dudarev, G.A. Botton, S.Y. Savrasov, Z. Szotek, W.M. Temmerman, and A.P. Sutton, Phys. Stat. Sol. (a) **166**, 429 (1998).
25. M. D. Towler, N. L. Allan, N. M. Harrison, V. R. Saunders, W. C. Mackrodt and E. Apra, Phys. Rev. B**50**, 5041 (1994).
26. T. Sasaki, Phys. Rev. **B54**, R9581 (1996).
27. G. A. Sawatzky and J. W. Allen, Phys. Rev. Lett. **53**, 2339 (1984).
28. Z. Szotek, W. M. Temmerman and H. Winter, Phys. Rev. Lett. **72**, 1244 (1994).
29. A. Svane, Phys. Rev. Lett. **72**, 1248 (1994).
30. W.M. Temmerman, A. Svane, Z. Szotek and H. Winter, in "Electronic Density Functional Theory: Recent Progress and New Directions", Eds. J.F. Dobson, G. Vignale and M.P. Das, Plenum Press, New York, 1998.
31. S.V. Beiden, W.M. Temmerman, Z. Szotek and G.A. Gehring, Phys. Rev. Lett. **79**, 3970 (1997).
32. The errorbars in the quoted experimental transition pressures are the present authors estimates based on the hysteresis loop observed in the experimental PV curves. The quoted volume changes are relative to the equilibrium volume and taken at the average transition pressure.
33. I. Vedel, A. M. Redon, J. Rossat-Mignod, O. Vogt and J. M. Leger, J. Phys. C **20**, 3439, (1987).
34. N. Mori, Y. Okayama, H. Takahashi, Y. Haga and T. Suzuki, Physica **B186-188**, 444 (1993).
35. A. Werner, H. D. Hochheimer, R. L. Meng and E. Bucher, Physics Lett. **97A**, 207, (1983).
36. J. M. Leger, D. Ravot and J. Rossat-Mignod, J. Phys. C **17**, 4935, (1984).
37. J. M. Leger, K. Oki, J. Rossat-Mignod and O. Vogt, J. de Physique **46**, 889, (1985).
38. A. Svane, Z. Szotek, W.M. Temmerman and H. Winter, Solid State Commun. **102**, 473 (1997).
39. A. Svane, Z. Szotek, W.M. Temmerman, J. Lægsgaard and H. Winter, J. Phys. Condens. Matter **10**, 5309 (1998).
40. F. Hulliger, M. Landolt, H. R. Ott and R. Schmelczer, J. Low Temp. Phys. **20**, 269 (1975).
41. Y. Okayama, Y. Ohara, S. Mituda, H. Takahashi, H. Yoshizawa, T. Osakabe, M. Kohgi, Y. Haga, T. Suzuki and N. Mori, Physica **B186-188**, 531 (1993).
42. T. Chattopadhyay, Science **264**, 226 (1994).
43. M. Kohgi, T. Osakabe,K. Kakurai,T. Suzuki, Y. Haga, and T. Kasuya, Phys. Rev. B**49**, 7068 (1994).
44. Y. Haga, A. Uesawa, T. Terashima, S. Uji, H. Aoki, Y. S. Kwon, and T. Suzuki, Physica **B206-207**, 792 (1995).
45. T. Terashima, S. Uji, H. Aoki, W. Joss, Y. Haga, A. Uesawa, and T. Suzuki, Phys. Rev. B **55**, 4197 (1997).
46. H. Kumigashira, S.-H. Yang, T. Yokoya, A. Chainani, T. Takahashi, A. Uesawa and T. Suzuki, Phys. Rev. B **55**, R3355 (1997).